

# Numerical and Experimental Study of NCN Mechanism: Contribution to Prompt-NO Formation

*N. Lamoureux\*, S. Canneaux, A. El Bakali, F. Louis, J.F. Pauwels, P. Desgroux*

*PC2A UMR CNRS 8522, University of Lille 1, France.*

## Abstract

The well-known prompt-NO mechanism initiated by the reaction between the CH radicals and N<sub>2</sub> has been recently re-considered and yields the formation of NCN + H. Using the cavity ring down spectroscopy (CRDS) combined with Laser Induced Fluorescence (LIF), the NCN radicals together with CH and NO species have been quantitatively measured in a rich premixed CH<sub>4</sub>/O<sub>2</sub>/N<sub>2</sub> flame stabilized at low pressure. Based on the experimental species profiles, and with the help of quantum chemistry tools for examining kinetic parameters of NCN channels especially via C<sub>2</sub>O radical, the NCN sub-mechanism has been modified in the GDFkin<sup>®</sup>3.0\_NCN mechanism.

## Introduction

It is now well admitted that the prompt-NO formation is mainly initiated according to the reaction: CH + N<sub>2</sub> = NCN + H. El Bakali et al. [1] introduced this key reaction in the mechanism GDFkin<sup>®</sup>3.0\_NCN. Very recently, the rate constant has been re-examined using experimental measurements [2] and theoretical calculations [3]. Few studies have carried out NCN measurements in laminar low-pressure flames [4,5] using Laser Induced Fluorescence (LIF). Recently, we have been able to quantitatively measure the NCN radical in a rich CH<sub>4</sub>/O<sub>2</sub>/N<sub>2</sub> flame [6] using the cavity ring down spectroscopy (CRDS) combined with LIF. Examination of 1/ the kinetic data and 2/ the different assumptions for the prompt-NO formation (C<sub>2</sub>O route, ...) shows that the chemistry of the radical NCN suffers from lack of data.

The present work aims to contribute to a better understanding of the prompt-NO mechanism by reporting 1/ an experimental study consisting in the quantitative concentration profiles of NCN, CH and NO species in a low pressure CH<sub>4</sub>/O<sub>2</sub>/N<sub>2</sub> flame and 2/ a modification of the NCN sub-mechanism in GDFkin<sup>®</sup>3.0\_NCN. In addition quantum chemistry tools have been used to examine kinetic parameters of NCN channels especially via C<sub>2</sub>O radical.

## Experimental Setup

Experiments were performed in a 0.6 CH<sub>4</sub> / 0.96 O<sub>2</sub> / 3.29 N<sub>2</sub> (slpm) laminar, premixed flame ( $\phi = 1.25$ ) stabilized at 5.3 kPa (40 torr) on a 6-cm-diameter bronze McKenna burner. The burner is vertically mobile in a stainless enclosure. The pressure was controlled via a 0-13.3 kPa pressure gauge. The facility is equipped with six optical accesses ports (opposite 2 by 2 at 90° and 45° from the laser axis) for laser diagnostics.

The temperature profile has been determined from a two-line atomic fluorescence technique (TLAF) [7]. Close to the burner, where the TLAF technique is not applicable, the temperature profile was measured using a commercial type-K thermocouple.

The laser system consists of a frequency-doubled Quantel Nd:YAG laser pumping a dye laser. Wavelengths around 329 nm (corresponding to the A<sup>3</sup>Π<sub>u</sub>-X<sup>3</sup>Σ<sub>g</sub><sup>-</sup> transition in NCN) were provided by doubling the fundamental dye (LDS698 + DCM diluted in methanol) radiation pumped with the 532 nm. Wavelengths around 317 nm (corresponding to the C<sup>2</sup>Σ<sup>+</sup>←X<sup>2</sup>Π(0,0) transition of the CH radicals) were provided by doubling the fundamental dye (Rh640 + DCM diluted in methanol) radiation pumped with the 532 nm. The 6-ns duration pulse had a bandwidth around 0.15 cm<sup>-1</sup>. For the NO excitation, wavelengths around 225 nm (corresponding to the A<sup>2</sup>Σ<sup>+</sup>←X<sup>2</sup>Π(0,0) of the NO) were obtained by mixing the frequency-doubled output of the dye laser (Rh590 + Rh610 diluted in methanol) with the residual infrared radiation of the YAG laser. The resulting FWHM linewidth was around 1 cm<sup>-1</sup>. Dye laser wavelengths were systematically calibrated with LIF-excitation spectrum from LIFBASE software [8]. The laser energy fluctuations were monitored by a postflame photodiode (which was used as the trigger source of the data acquisition).

For the LIF measurements, the laser beam was injected unfocused into the burner enclosure. At the exit, a Brewster window was set in order to minimize the laser reflections. The LIF signal was collected at 90°. The spatial resolution along the vertical flame axis was achieved by imaging the central portion of the laser beam on the horizontal slit (10-mm-height, 250-μm-width, parallel to the axis burner) of a 0.25-m spectrometer by a two-lens system at f/4. The output slit was adjusted to provide the appropriate collection bandwidth in order to collect the fluorescence from all the rotational transitions according to the dispersed LIF spectrum. The fluorescence signals were collected with a 1.5 ns rise-time Photonis XP2020Q photomultiplier tube. The fluorescence and laser intensity signals were simultaneously time-resolved, averaged and stored by a digital scope (Lecroy 9354A, 8-bit, 500-MHz, 1-GS/s). The collected traces were processed using Labview7.1 software. LIF signals were measured at their temporal peak to minimize the effect of quantum yield variation along the flame. LIF signal led to the rotational population N(J'') easily converted in total density

\* Corresponding author: [nathalie.lamoureux@univ-lille1.fr](mailto:nathalie.lamoureux@univ-lille1.fr)  
Proceedings of the European Combustion Meeting 2009

number  $n$  using the Boltzmann fraction  $f_B(J'',T)$ . Comparison with modelling data being based on the species mole fraction, this last one is derived from the total number of density and the ideal gas law. At each height above the burner (HAB) (250- $\mu\text{m}$  step), the PMT signal was averaged over 255 pulses before being processed. Measurements profiles have been performed several times in the same conditions to ensure repeatability. The calibration of the LIF signal was then performed in the zone where the species concentration is maximal in the flame. So, it was performed at the peak value for the CH and NCN calibration, and at 20 mm above the burner for NO calibration.

For the CRD measurements, the laser beam was shaped with a system consisting of a 100- $\mu\text{m}$  pinhole aperture and two 100-mm focal lenses in order to match approximately the TEM<sub>00</sub> transverse mode of the CRD cavity [9]. The 420-mm length CRD cavity consisted of 2 high reflectivity mirrors (25-mm diameter, 250-mm radius of curvature, R=99.72% at 329 nm, R=99.70% at 317 nm). A UG11 filter was placed in between the rear mirror of the CRD cavity and the PMT (XP2020Q). The signal was recorded using the digital scope triggered using a photodiode, averaged over 255 pulses and processed in order to measure the cavity decay time,  $\tau(\lambda)$ , using a fast exponential fitting algorithm for real-time instrumentation [10] with Labview7.1. The fitting procedure was performed over 920 points which represents a duration of 1840 ns (i.e. around  $4 \times \tau$ ), with a resulting standard deviation lower than 0.2%. The decay time can be regarded as:

$$\tau(\lambda) = \frac{l_{cav}}{c((1-R(\lambda)) + \sigma(\lambda, T)nl_s + L_{fl}(\lambda))} = \frac{l_{cav}}{c} \frac{1}{L(\lambda)}$$

where  $R(\lambda)$  is the mirror reflectivity,  $\sigma(\lambda, T)$  is the absorption cross-section of the sample at temperature T and  $l_s$  is the flame diameter.  $L_{fl}(\lambda)$  includes all scattering and absorption losses or thermal deflection resulting from insertion of flame into the cavity [9,11],  $c$  is the speed of light and  $l_{cav}$  is the length of the cavity, and  $L(\lambda)$  is the loss per pass in the cavity. In flame conditions, the absorption due to the species (i.e. the net losses/pass) is determined by measuring the OFF- and ON- resonance cavity decay times, respectively  $\tau_{OFF}$  and  $\tau_{ON}$ , according to:

$$\sigma(\lambda, T)nl_s = \frac{l_{cav}}{c} \left( \frac{1}{\tau_{ON}} - \frac{1}{\tau_{OFF}} \right).$$

The OFF-resonance decay time is implicitly considered not being affected by additional perturbations or species absorption. The standard deviation of the cavity decay time was 0.5 ns, which corresponds to a sensitivity limit of 7 ppm/pass.

## Experimental Results

NCN-LIF signal was obtained by exciting the bandhead of the  $A^3\Pi_u - X^3\Sigma_g^-$  transition of the NCN radical at 329.13 nm with a collection bandwidth of 8 nm, in order to collect the fluorescence from all the rotational transitions according to the dispersed LIF spectrum. Laser energy was reduced to 60  $\mu\text{J}/\text{pulse}$  for a

laser beam of 0.5  $\text{cm}^2$ . Because the NCN radical fluoresces almost entirely at the exciting wavelength [12], the collected signal was perturbed by laser scattering in the enclosure. In order to minimize this background noise, the LIF signal was measured by integrating the signal 1 ns after the laser pulse for 12 ns. Simultaneously, the fluorescence lifetime was measured (between 90% and 10% of the amplitude of the signal delivered by the PMT) in order to verify that the quenching does not vary along the NCN profile. Due to the very low NCN concentration in the methane flame as previously reported [6], the calibrating step using CRD was performed in a rich ( $\phi=1.25$ ) acetylene/ $\text{O}_2/\text{N}_2$  flame where the NCN profile was determined from the net losses measurements (43 ppm/pass). Thank to spectral simulation [13], the absorption cross-section of the NCN radical was determined to be equal to  $9.4 \cdot 10^{-7} \text{ cm}^2/\text{molecule}$  at 1830 K [6], allowing the net losses profiles to be converted in mole fraction to be 360 ppb with an overall accuracy of 25% at the peak value. The relative LIF signals between the methane and acetylene flames yields a NCN peak value of 170 ppb with an accuracy of 25%. This procedure allows to improve by more than a factor of the 2 the accuracy of the measurements previously reported.

CH-LIF measurements were performed by using a pre-dissociative state ( $C^2\Sigma^+ \leftarrow X^2\Pi(0,0)$  transition) of CH near 315 nm, according to an excitation/detection scheme previously used in the lab [14,15]. The line  $P_2(8)$  near 316.7 nm was selected for the CH excitation and the fluorescence was collected in the entire Q-branch at 314.7 nm with a narrow bandwidth of 3.0 nm selected by the spectrometer in order to reject all the interference due to flame emission. LIF signal was calibrated from the absorptivity measurement (using CRD) at the peak concentration location by scanning the laser around the  $P_1(8)$  and  $P_2(8)$  lines. Using a deconvolution method and considering the absorption constant across the flame diameter (one-dimensional flame), the absolute number density of the excited rotational level ( $N''=8$ ) was determined. Knowing the temperature at the measured location ( $T=1830 \text{ K}$ ), the CH-peak mole fraction was determined as being  $(7.5 \pm 0.6)$  ppm in the flame.

NO-LIF measurements in flames were performed by excitation of the  $A^2\Sigma^+ \leftarrow X^2\Pi(0-0)$  band near 225.6 nm ( $Q_2(27)$  line) and the collection of the  $A^2\Sigma^+ \rightarrow X^2\Pi(0-2)$  band around 246 nm with a bandwidth of 8 nm. The excitation range is possibly disturbed by  $\text{O}_2$  Schumann-Runge bands and caution has been paid to prevent from these backgrounds by recording OFF-resonance signals [16]. The relative NO profiles were determined from the difference between the ON- and the OFF- resonance signals. In the burned gases (HAB=20 mm), the LIF signal was calibrated following a seeding procedure in a stoichiometric methane/ $\text{O}_2/\text{N}_2$  flame where NO was gradually added from 0 to 700 ppm in the premixed gases, yielding a NO mole fraction in the studied flame of  $(26.5 \pm 2.7)$  ppm.

## Modelling

Premix code of the Chemkin-II package [17,18] was used during this work in order to perform modelling computations. Kinetic analysis is essentially based on the rate of production and consumption. All computations have been performed using experimental temperature profile. The mass flux is computing with respect of the standard volumetric flow rate and the burner surface area. The detailed mechanism GDFkin<sup>®</sup>3.0\_NCN [1], fully validated for natural gas oxidation in presence of N-species [1,14], was used for the species profiles simulation. It takes into account the new route of NCN contribution in the prompt NO formation. This model involves 883 reactions and 121 species.

### NCN route

In the present work, the rate constants of the reactions involving the NCN radicals have been updated in agreement with the recent determinations, as reported in Table 1. The rate constant of the reaction  $\text{CH} + \text{N}_2 = \text{NCN} + \text{H}$  (which has been confirmed from theoretical calculations [3]) is issued from experimental determination in shock tubes [2]. The rate constant of the reaction  $\text{NCN} + \text{H} = \text{HCN} + \text{N}$  issued from theoretical calculations [19] was confirmed from experiments [2]. The other rate constants were calculated by theoretical chemistry by Lin's group [20,21,22].

Reactions	Rate constant ( $\text{cm}^3 \cdot \text{mol}^{-1}$ , K)
$\text{CH} + \text{N}_2 = \text{NCN} + \text{H}$	$6.03 \times 10^{12} \exp(-11150/T)$ [2]
$\text{NCN} + \text{H} = \text{HCN} + \text{N}$	$1.89 \times 10^{14} \exp(-4234/T)$ [19]
$\text{NCN} + \text{O}_2 = \text{NCO} + \text{NO}$	$3.80 \times 10^9 T^{0.51} \exp(-12377/T)$ [20]
$\text{NCN} + \text{O} = \text{CN} + \text{NO}$	$2.55 \times 10^{13} T^{0.15} \exp(17/T)$ [21]
$\text{NCN} + \text{OH} = \text{HCN} + \text{NO}$	$4.71 \times 10^{10} T^{0.44} \exp(-2013/T)$ [22]

**Table 1.** Rate constants updated for the reactions involved in the NCN sub-mechanism in GDFkin<sup>®</sup>3.0\_NCN.

### Methylene route

Examination of the methylene ( $^1\text{CH}_2$ ) role on the prompt-NO formation, after Williams et al. [23] has also been considered. The  $\text{CH}_2\text{N}_2$  and  $\text{HCNN}$  sub-mechanisms have been introduced. Their impact on the simulated species implied in the prompt-NO mechanism was found insignificant. Therefore previous sub-mechanisms were not included in the present version of the mechanism. The role of methylene was examined in a GRI3.0-based mechanism [24], showing no effect in the case of the rich mixture flame. Its role was indeed postulated to be effective in case of lean mixtures.

### C<sub>2</sub>O route

Another route leading to prompt-NO was also postulated by Williams et al. [25] and relies on the Konnov5.0 mechanism [26]. This route consists in NCN initiation from the reaction  $\text{C}_2\text{O} + \text{N}_2 = \text{NCN} + \text{CO}$ . It was considered in order to better predict the effect of both equivalence ratio and fuel on the prompt-NO formation. One has to note that in the initial GDFkin<sup>®</sup>3.0\_NCN mechanism,  $\text{C}_2\text{O}$  radicals are produced via the sole reaction:  $\text{C}_2 + \text{OH} = \text{C}_2\text{O} + \text{H}$ , contrary to Konnov's where

an additional reaction for the  $\text{C}_2\text{O}$  formation is given:  $\text{HCCO} + \text{OH} = \text{C}_2\text{O} + \text{H}_2\text{O}$ . The introduction of the reaction  $\text{C}_2\text{O} + \text{N}_2 = \text{NCN} + \text{CO}$  in the GDFkin<sup>®</sup>3.0\_NCN mechanism does not modify the NCN or NO profiles. Then, the subsequent reaction  $\text{HCCO} + \text{OH} = \text{C}_2\text{O} + \text{H}_2\text{O}$ , according to Konnov [26], was introduced. Due to this last reaction, the  $\text{C}_2\text{O}$  radicals are obviously produced more than twice, yielding an increase in the NCN peak value (due to the former reaction) and NO mole fraction. Furthermore decreasing the rate constant of the reaction  $\text{C}_2\text{O} + \text{N}_2 = \text{NCN} + \text{CO}$  can diminish the quantity of prompt-NO predicted in the flame as confirmed recently by Konnov [27] who obtained a good agreement between simulated and experimental NO profiles in different atmospheric premixed flames.

However accurate data (theoretical or experimental) concerning the pathways of the  $\text{C}_2\text{O}$  radical and the rate constant of the reaction  $\text{C}_2\text{O} + \text{N}_2 = \text{NCN} + \text{CO}$  are still completely lacking. At this stage, we considered that it was premature to go further in the adjustment of the rate constant. A preliminary theoretical study has been favoured here to determine the reaction pathways subsequent to the reaction between  $\text{C}_2\text{O}$  and  $\text{N}_2$ .

Density Functional Theory (DFT) calculations were performed using the GAUSSIAN03 [28] software package. Reactants, molecular complexes, products, and transition state (TS) structures were fully optimized at HF-DFT (B3LYP) [29] level of theory using the Dunning's correlation consistent double-zeta plus polarization aug-cc-pVDZ [30] basis set. All TSs have been characterized by one imaginary frequency (first-order saddle points) on the Potential Energy Surface (PES). Special care was taken to determine Minimum Energy Pathways (MEPs), performing Intrinsic Reaction Coordinate analyses (IRC) [31], in order to confirm that a specific TS connects the different local minima. Vibrational frequencies were determined within the harmonic approximation, at the same level of theory as for geometries.

The reaction of  $\text{C}_2\text{O}$  radicals with  $\text{N}_2$  is a multichannel mechanism:



The  $\text{N}_2$  molecule approaches the  $\text{C}_2\text{O}$  radical and reacts through an addition to form a molecular complex  $\text{NNCCO}$  (MC1-2). From this latter, two channels have been characterized, Fig. 1. The channel (a) is not energetically favoured. The channel (b) seems to be the most energetically favoured at the B3LYP/aug-cc-pVDZ level of theory. The PES has to be completed in order to take into account other pathways (yielding  $\text{NCO} + \text{CN}$  for instance). Higher correlated methods will be used in order to confirm the observed trends. After elucidating the mechanism, rate constants will be estimated. This preliminary study, at 0 K, shows that the channel yielding  $\text{NCN} + \text{CO}$  is not favoured compared with the  $\text{NNC} + \text{CO}$  channel. It is premature to make any conclusion about the tendency at higher temperature, and thus about the contribution of  $\text{C}_2\text{O}$  route to prompt-NO formation.

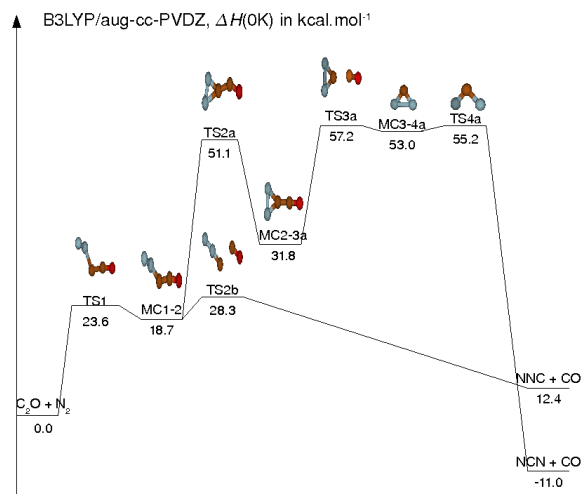


**Fig. 1.** Potential Energy Surface of the C<sub>2</sub>O + N<sub>2</sub> reaction system at the B3LYP/aug-cc-pVDZ level of theory (red: oxygen, blue: nitrogen, brown: carbon)

### Discussions

Experimental and simulated profiles of CH, NCN and NO are reported Figure 2. Modelling results from the initial GDFkin<sup>®</sup>3.0\_NCN mechanism show a fairly good agreement with the experimental profiles of CH and NO, which was expected since the mechanism has already been validated against these species profiles. The simulated NCN profile presents a peak value of about 30 ppb, much lower than the experimental results.

Using the revised version of the mechanism, one can note no change for the CH profile, the improvement of the simulated NCN profile (with a peak value of 130 ppb), but the NO profile falls of 20%.

Care must be taken in the prompt-NO mechanism modifications (new reactions, rate constant adjustment). Up to now the CH radicals are always considered as the key species, so the modifications have to take into account not only the NO profiles but the CH and the NCN profiles. Prediction of CH and NO peak mole fractions obtained by the GRI3.0, Konnov5.0 or GDFkin<sup>®</sup>3.0\_NCN mechanisms are different as shown Figure 3 where the ratio of the simulated and experimental mole fractions of CH, NCN and NO are presented. In the present flame conditions, one can note that the CH peak value according to the GRI3.0 mechanism widely overestimates the experimental one, but the NO prediction is in good agreement with the experimental results. Considering the Konnov5.0 mechanism, both CH and NO are underestimated. The initial version of the GRI3.0 as well as Konnov5.0 mechanisms do not take into account the NCN route in the prompt-NO formation. The introduction of the 5 reactions reported in Table 1 generates an increase of the NO prediction unlike the observed diminishing using GDFkin<sup>®</sup>3.0\_NCN mechanism, Fig. 3(b). But the NCN peak value is in all cases quite good predicted against the experimental value.

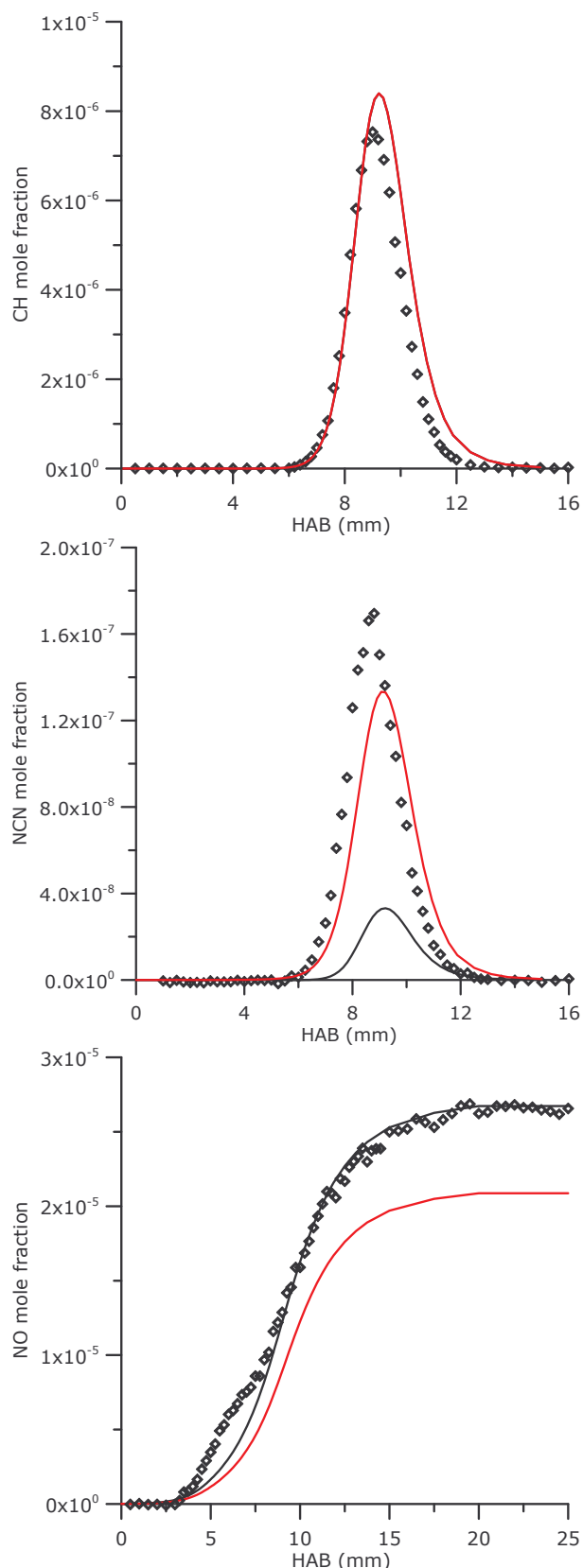


**Fig. 2.** Species profiles measured in the rich ( $\phi=1.25$ ) CH<sub>4</sub>/O<sub>2</sub>/N<sub>2</sub> flame (diamonds: exp.) compared to simulated ones: black line: GDFkin<sup>®</sup>3.0\_NCN; red line: revised mechanism.

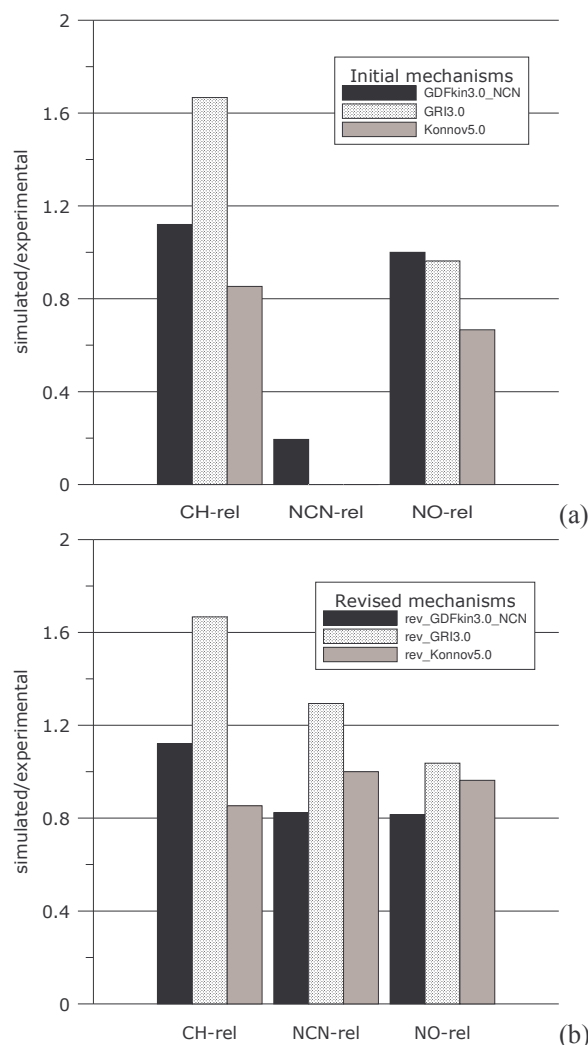


**Fig. 3.** Ratio of simulated peak values of CH, NCN and NO species relatively to the experimental ones measured in the rich  $\text{CH}_4/\text{O}_2/\text{N}_2$  flame, using different mechanisms. (a) without any modification, (b) with the 5 reactions and their rate constant listed in table 1.

## Conclusions

In a rich  $\text{CH}_4/\text{O}_2/\text{N}_2$  flame, CH, NCN and NO profiles have been quantitatively measured using laser diagnostics (LIF/CRDS). Modelling profiles have been performed based on the GDFkin<sup>®</sup>3.0\_NCN mechanism. Both experimental and numerical results show the importance of the NCN radicals in the prompt-NO formation through the key reaction  $\text{CH} + \text{N}_2 = \text{NCN} + \text{H}$ . Consequently, the rate constant of the reaction involving the NCN radical have been updated according to recent experimental and theoretical results. This leads to an improvement of the NCN profile prediction compared to the experimental one.

Comparison with different detailed mechanism (GRI3.0 and Konnov5.0) has been performed and completed with the introduction of the NCN sub-mechanism, Table 1. None of the three mechanisms is perfect.

NCN radical can be simulated in good agreement with experimental results. Present work highlights that the rate constants of the reactions involved in the prompt-NO formation suffer from lack of data. Before

proceeding to further modifications in the mechanism, we aimed to complete the database of species involved in the prompt-NO formation and pursue our efforts in theoretical chemistry to assess the relevance of reactions to be considered.

## Acknowledgements

The authors are grateful to I. Burns (Dpt. of Chemical Engineering, Univ. of Cambridge) for providing temperature profile using TLAf technique. This work was supported by the ANR program BLAN08-3\_350752 and by the Air Quality Program of IRENI (Institut de Recherche en ENvironnement Industriel). The authors thank the Nord-Pas de Calais Region and the European Funds for Regional Economic Development for their financial support.

## References

- 1 A. El Bakali, L. Pillier, P. Desgroux, B. Lefort, L. Gasnot, J.F. Pauwels, I. da Costa, Fuel 85 (7-8) (2006) 896-909
- 2 V. Vasudevan, R.K. Hanson, C.T. Bowman, D.M. Golden, D.F. Davidson, J. Phys. Chem. A 111 (46) (2007) 11818-11830
- 3 L.B. Harding, S.J. Klippenstein, J.A. Miller, J. Phys. Chem. A 112 (3) (2008) 522-532
- 4 G.P. Smith, Chem. Phys. Letters 367 (5-6) (2003) 541-548
- 5 J.A. Sutton, B.A. Bradley, J.W. Fleming, Combust. Flame 153 (3) (2008) 465-478
- 6 N. Lamoureux, X. Mercier, C. Western, J.F. Pauwels, P. Desgroux, Proc. Combust. Inst. 32 (2009) 937-944
- 7 J. Hult, I.S. Burns, C.F. Kaminski, Proc. Combust. Inst. 30 (2005) 1535-1543
- 8 J. Luque, D.R. Crosley, LIFBASE: Database and spectral simulation (version 1.5), SRI International Report MP 99-009, 1999
- 9 X. Mercier, E. Therssen, J.F. Pauwels, P. Desgroux, Combust. Flame 124 (4) (2001) 656-667
- 10 D. Halmer, G. von Basum, P. Hering, M. Mürtz, Rev. Sci. Instrum. 75 (6) (2004) 2187-2191
- 11 R. Evertsen, J. A. Van Oijen, R. T. E. Hermans, L. P. H. De Goey, J. J. Ter Meulen, Combust. Flame 132 (1-2) (2003) 34-42
- 12 G.P. Smith, Chem. Phys. Letters 367 (5-6) (2003) 541-548
- 13 C. M. Western, PGOPHER, a Program for Simulating Rotational Structure, University of Bristol, <http://pgopher.chm.bris.ac.uk>
- 14 L. Pillier, A. El Bakali, X. Mercier, A. Rida, J.-F. Pauwels, P. Desgroux, Proc. Combust. Inst. 30 (2005) 1183-1191
- 15 C. Moreau, E. Therssen, P. Desgroux, J.-F. Pauwels, A. Chappat, M. Barj, Appl. Phys. B 76 (5) (2003) 597-602
- 16 P. Desgroux, P. Devynck, L. Gasnot, J.-F. Pauwels, L.-R. Sochet, Appl. Optics 37 (21) (1998) 4951-4962
- 17 R.J. Kee, J.F. Grear, M.D. Smooke, J.A. Miller, A fortran program for modelling steady laminar one-dimensional premixed flames, Sandia report SAND85-8240, 1985
- 18 R.J. Kee, F.M. Rupley, J.A. Miller, Chemkin-II: A fortran chemical kinetics package for the analysis of gas phase chemical kinetics, Sandia report SAND89-80009B, 1989
- 19 L.V. Moskaleva, M.C. Lin, Proc. Combust. Inst. 23 (2000) 2393-2401
- 20 R.S. Zhu, M.C. Lin, Int. J. kinet. 37 (10) (2005) 593-598

- 
- <sup>21</sup> R.S. Zhu, M.C. Lin, J. Phys. Chem. A 111 (29) (2007) 6766-6771
- <sup>22</sup> R.S. Zhu, H.M.T. Nguyen, M.C. Lin, J. Phys. Chem. A 113 (1) (2009) 298-304
- <sup>23</sup> B.A. Williams, J.A. Sutton, J.W. Fleming, Proc. Combust. Inst. 32 (2009) 343-350
- <sup>24</sup> G.P. Smith, D.M. Golden, M. Frenklach, N.W. Moriarty, B. Eiteneer, M. Goldenberg, C.T. Bowman, R. Hanson, S. Song, W.G. Gardiner Jr, V. Lissianski, Z. Qin, Methane Kinetic Mechanism version 3.0 (1999)  
<http://www.me.berkeley.edu/gri-mech/>
- <sup>25</sup> B.A. Williams, J.W. Fleming, Proc. Combust. Inst. 31 (2007) 1109-1117
- <sup>26</sup> A.A. Konnov, Detailed Reaction Mechanism for Small Hydrocarbons Combustion, Release 0.5 (2000).  
<http://homepages.vub.ac.be/~akonnov/>
- <sup>27</sup> A.A. Konnov, Combust. Expl. Shock Waves 44 (5) (2008) 497-501
- <sup>28</sup> M.J. Frisch et al., GAUSSIAN 03, Revision D.01, Gaussian, Inc., Wallingford CT, 2004
- <sup>29</sup> (a) C. Lee, W. Yang, R. Parr, Phys. Rev. B 37 (1988) 785-789. (b) A. Becke, J. Chem. Phys. 98 (7) (1993) 5648-5652
- <sup>30</sup> (a) T.H. Dunning Jr, J. Chem. Phys. 90 (2) (1989) 1007-1023. (b) D.E. Woon, T.H. Dunning Jr, J. Chem. Phys. 98 (2) (1993) 1358-1371. (c) D.E. Woon, T.H. Dunning Jr, J. Chem. Phys. 100 (4) (1994) 2975-2988. (d) A.K. Wilson, D.E. Woon, K.A. Peterson, T.H. Dunning Jr, J. Chem. Phys. 110 (16) (1999) 7667-7676. (e) R.A. Kendall, T.H. Dunning, R.J. Harrison, J. Chem. Phys. 96 (9) (1992) 6796-6806
- <sup>31</sup> C. Gonzalez, H.B. Schlegel, J. Chem. Phys. 90 (4) (1989) 2154-2161